Title
Accuracy of subsurface temperature distributions computed from pulsed photothermal radiometry

Journal
Physics in Medicine and Biology, 43(9)

ISSN
0031-9155

Authors
Smithies, Derek J
Milner, Thomas E
Tanenbaum, B Samuel
et al.

Publication Date
1998-09-01

DOI
10.1088/0031-9155/43/9/002

Phys. Med. Biol. **43** (1998) 2453–2463. Printed in the UK PII: S0031-9155(98)86026-0

Accuracy of subsurface temperature distributions computed from pulsed photothermal radiometry

Derek J Smithies†‖, Thomas E Milner†, B Samuel Tanenbaum§, Dennis M Goodman§ and J Stuart Nelson†¶

† Beckman Laser Institute and Medical Clinic, University of California, Irvine, CA 92612, USA
‡ Harvey Mudd College, Claremont, CA 91711, USA
§ Lawrence Livermore National Laboratory, University of California, Livermore, CA 94550, USA

Received 15 July 1997, in final form 14 April 1998

Abstract. Pulsed photothermal radiometry (PPTR) is a non-contact method for determining the temperature increase in subsurface chromophore layers immediately following pulsed laser irradiation. In this paper the inherent limitations of PPTR are identified.

A time record of infrared emission from a test material due to laser heating of a subsurface chromophore layer is calculated and used as input data for a non-negatively constrained conjugate gradient algorithm. Position and magnitude of temperature increase in a model chromophore layer immediately following pulsed laser irradiation are computed. Differences between simulated and computed temperature increase are reported as a function of thickness, depth and signal-to-noise ratio (SNR).

The average depth of the chromophore layer and integral of temperature increase in the test material are accurately predicted by the algorithm. When the thickness/depth ratio is less than 25%, the computed peak temperature increase is always significantly less than the true value. Moreover, the computed thickness of the chromophore layer is much larger than the true value.

The accuracy of the computed subsurface temperature distribution is investigated with the singular value decomposition of the kernel matrix. The relatively small number of right singular vectors that may be used (8% of the rank of the kernel matrix) to represent the simulated temperature increase in the test material limits the accuracy of PPTR. We show that relative error between simulated and computed temperature increase is essentially constant for a particular thickness/depth ratio.

1. Introduction

Pulsed photothermal radiometry (PPTR) is a non-contact method for obtaining information on subsurface chromophores in a test material. A fast infrared detector is used to measure increase in infrared emission at the test material surface following pulsed laser irradiation (Milner *et al* 1995a, b). From the time record of infrared emission increase, estimates of thickness and depth of subsurface chromophores can be computed. Reported applications of PPTR include the evaluation of surface coating thickness in industrial components (Crostack *et al* 1989), the identification of subsurface microcracks in aircraft structures (Favro *et al* 1993), the determination of the optical absorption coefficients in human arteries (Long and Deutsch 1987) and biliary calculi (Long *et al* 1987) and the characterization of port wine

‖ Also at: Physics and Astronomy Department, University of Canterbury, Christchurch, New Zealand.
¶ Author to whom correspondence should be addressed.

0031-9155/98/092453+11$19.50

stain birthmarks (Jacques *et al* 1993). Analysis of the performance of PPTR to accurately compute the size and position of blood vessels in a port wine stain (PWS) is of particular interest. Efficacy of the pulsed laser treatment of PWS can be improved if the size and position of blood vessels is known (Kimel *et al* 1994).

While several authors have reported on the use of PPTR (Jacques *et al* 1993, Vitkin *et al* 1994, Milner *et al* 1995a, b, 1996a, b), theoretical limits on the accuracy of the estimated position and magnitude of the temperature increase in discrete laser-heated subsurface chromophores have not been proposed or established. In this paper, we investigate the fundamental limitations of PPTR.

A non-negatively constrained conjugate gradient algorithm is used to compute the position and magnitude of temperature increase within a test material from the time record of infrared emission following pulsed laser irradiation.

Results from the non-negatively constrained conjugate gradient algorithm are verified using a singular value decomposition (SVD) analysis of the PPTR kernel function $K(t, z)$. Since each model temperature increase may be resolved as a superposition of variable number of right singular vectors of the PPTR kernel matrix, limitations on the computed thickness, depth and magnitude of temperature increase are established for various signal-to-noise ratios (SNR).

2. Method

The skin model (figure 1) contains a single chromophore layer. The laser spot diameter at the model surface is assumed to be large relative to the thermal and optical diffusion lengths so that heat transport is only considered along the depth (z) axis. Immediately following pulsed laser irradiation ($t = 0$), the simulated temperature increase within the skin model is given by $\Delta T_s(z)$ (°C). The relationship between increase in PPTR signal, ΔS (°C), and ΔT_s is given by a Fredholm integral of the first kind (equation (1)) (Milner *et al* 1995a)

$$\Delta S(t) = \int_z \Delta T_s(z) K(t, z)\, \mathrm{d}z + n(t) \tag{1}$$

where time is represented by t (s) and distance into the tissue, measured normal to the surface, is given by z (mm). Including effects of infrared emission and a convective boundary condition, the kernel function $K(t, z)$ (Milner *et al* 1995a), is

$$K(t, z) = \frac{\mu_{ir}}{2} \exp\left(\frac{-z^2}{4Dt}\right) \left[\mathrm{erfcx}(\mu_+(t, z)) + \mathrm{erfcx}(\mu_-(t, z)) + \frac{-2h}{h - \mu_{ir}} (\mathrm{erfcx}(\mu_+(t, z)) - \mathrm{erfcx}(\mu_1(t, z))) \right] \tag{2}$$

where $\mathrm{erfcx}(u) = \exp(u^2) \times \mathrm{erfc}(u)$ is the exponential complementary error function. Functions $\mu_\pm(t, z)$ and $\mu_1(t, z)$ are defined as

$$\mu_\pm(t, z) = \mu_{ir}\sqrt{Dt} \pm \frac{z}{2\sqrt{Dt}} \tag{3}$$

$$\mu_1(t, z) = h\sqrt{Dt} + \frac{z}{2\sqrt{Dt}}. \tag{4}$$

Signal noise, $n(t)$, an inherent component of the system is taken as a zero-mean, white, Gaussian distributed function. The signal-to-noise variance $\langle n^2 \rangle$ is related to the SNR of the infrared detection system

$$\mathrm{SNR} = \langle \Delta S(t) \rangle / \langle n^2 \rangle^{1/2} \tag{5}$$

where $\langle x \rangle$ represents a time average of the quantity x. Physical constants used in the skin model (from Robertson and Williams 1971, Duck 1990, Incropera and DeWitt 1985) are: thermal diffusivity D (1.1×10^{-2} mm^2 s^{-1}), infrared absorption coefficient μ_{ir} (45×10^{-2} mm^{-1}), and free convection heat-transfer coefficient, h (0.03 mm^{-1}).

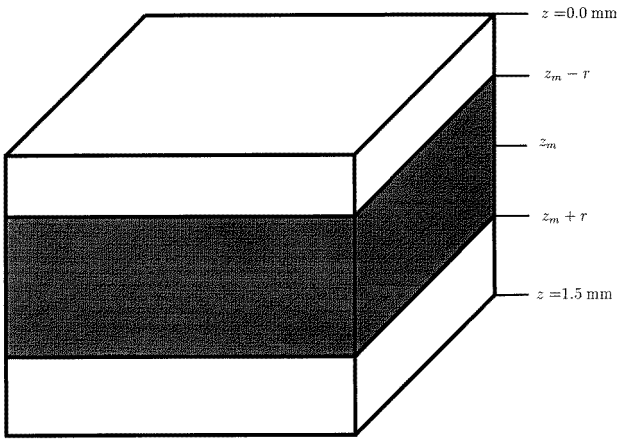

Figure 1. Skin model. Mean chromophore layer depth is z_m (μm), and thickness $2r$ (μm). Maximum depth of the simulation is 1.5 mm.

A tophat shaped simulated temperature increase distribution (equation (6)) was used to represent the temperature change within tissue. Such a temperature increase distribution is difficult to reconstruct since it contains abrupt changes in value. Consequently this temperature distribution provides an excellent test for the reconstruction algorithm and any deficiencies will become apparent

$$\Delta T_{st}(z) = \begin{cases} T_0 & z \geqslant z_m - r \text{ and } z \leqslant z_m + r \\ 0 & \text{otherwise.} \end{cases} \tag{6}$$

The PPTR signal from the model, ($\Delta S(t)$), was determined from

$$\Delta S(t) = V(t, z_m - r) - V(t, z_m + r) + n(t) \tag{7}$$

where

$$V(t,z) = \frac{T_0}{2} \exp\left(\frac{-z^2}{4Dt}\right) \left[\operatorname{erfcx}(\mu_+(t,z)) - \operatorname{erfcx}(\mu_-(t,z)) + \frac{2}{h - \mu_{ir}} (\mu_{ir} \operatorname{erfcx}(\mu_1(t,z)) - h \operatorname{erfcx}(\mu_+(t,z))) \right] \tag{8}$$

and derived from equation (1).

Computation of temperature increase in the skin model, given the PPTR signal as input data, is a severely ill-posed inverse problem. The problem is converted to a matrix equation and vector quantities representing $\Delta S(t)$ and $\Delta T(z)$ are denoted by boldface symbols $\Delta \boldsymbol{S}$ and $\Delta \boldsymbol{T}$. A non-negatively constrained conjugate gradient algorithm (see, for example, Goodman *et al* 1993) was used to compute the temperature increase within skin at $t = 0$. Briefly, this iterative method computes an ith estimate for the temperature increase within skin ($\Delta \boldsymbol{T}_{cg}(i)$) (initially a null field for $i = 0$) and the corresponding PPTR signal. $\Delta \boldsymbol{T}_{cg}(i)$ is compared with $\Delta \boldsymbol{S}$, and a revised estimate of ($\Delta \boldsymbol{T}_{cg}(i)$) is computed based upon conjugate

gradient direction. As temperature increase within skin is always positive, the solution is constrained so that negative values are not allowed ($\Delta \boldsymbol{T}_{cg}(i) \geqslant 0$).

The iterative process is terminated when the difference between the computed PPTR signal and $\Delta \boldsymbol{S}$ is less than the noise level (Groetsch 1984) or the difference ceases to change between successive iterations, or a preset number of iterations have been exceeded (Goodman *et al* 1993, Frank and Friedman 1993, Stone and Brooks 1990).

In our simulations, 256 uniformly spaced nodes were used to represent temperature increase in a 1.5 mm tissue depth. PPTR signal over a 3 s period immediately following pulsed laser irradiation was stored in a 512-element array.

3. Results

Computed temperature increase ($\Delta \boldsymbol{T}_{cg}$) was calculated (figure 2) after 100 iterations of the non-negatively constrained conjugate gradient algorithm for $z_m = 0.5$ mm and thicknesses ($2r$) between 0.032 and 0.5 mm. Error in the computed peak temperature increase was less than 15% for chromophore layers of thicknesses 0.25 and 0.50 mm and increased to 77% for the thinnest chromophore layer ($2r = 0.032$ mm). Note, however, that the depth z_m and $\int \Delta \boldsymbol{T}_{cg}\, \mathrm{d}z$ are still predicted accurately, even when the computed peak temperature increase is much less than T_0.

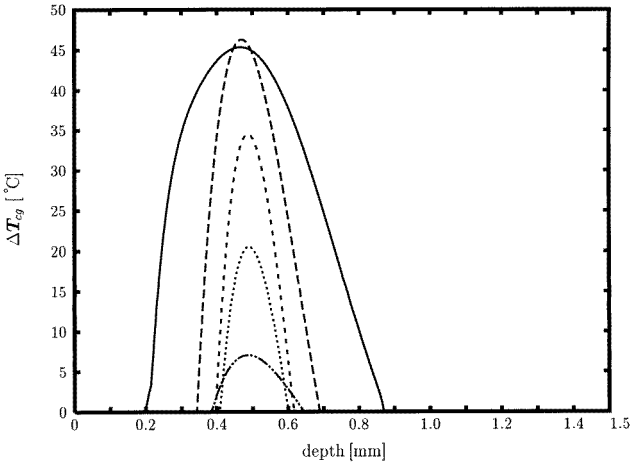

Figure 2. Computed temperature increase in skin model immediately following pulsed laser irradiation. Chromophore layer thicknesses are 0.5 mm (——), 0.25 mm (– – –), 0.125 mm (- - - -), 0.063 mm (· · · · · ·) and 0.032 mm (— · · —), at depth 0.5 mm. T_0 was set to 40 °C.

In each of the following simulations results were obtained after 100 iterations of the non-negatively constrained conjugate gradient algorithm, and regularized by early termination (Milner *et al* 1995a). For one particular $\Delta \boldsymbol{T}_{ts}$, repeated solutions of equation (1) yields a slight variation in the computed temperature increase ($\Delta \boldsymbol{T}_{cg}$), because $\Delta \boldsymbol{S}$ contains a noise component, $\boldsymbol{n}$. Thus, 20 inversions for each simulated temperature increase were computed and subsequent plots show mean and standard deviation of the displayed values.

The effect of source chromophore layer thickness is shown for $z_m = 0.2$ mm (figure 3). The computed peak temperature increase to T_0 is reported for three values of T_0 (5, 10 and 40 °C), and the chromophore layer thickness $2r$ is between 0.025 and 0.30 mm. When the chromophore layer thickness is greater than 0.1 mm, the computed peak temperature

increase differs from T_0 by less than 20%. As the chromophore layer thickness increases, the difference between the computed peak temperature increase and T_0 becomes less. For values of $2r < 0.1$ mm, the difference increases as the thickness of the source chromophore layer decreases.

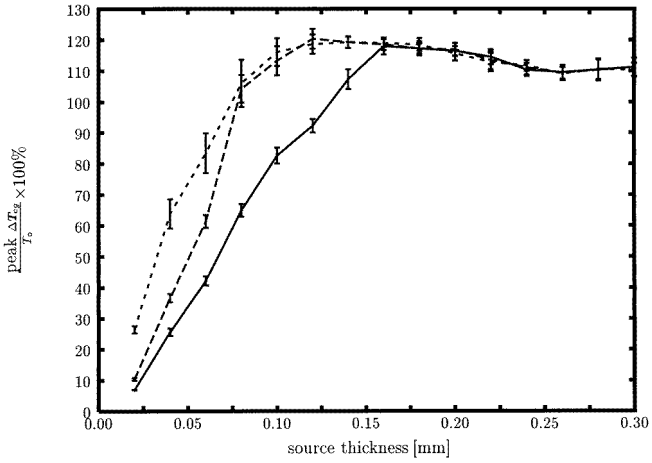

Figure 3. Ratio of computed peak temperature increase and T_0, for a chromophore layer of variable thickness at a depth of 0.2 mm. Chromophore layer temperatures used: 5 °C (——), 10 °C (– – –) and 40 °C (- - - -).

The thickness/depth ratio has a significant effect on computed temperature increase (figure 4). Chromophore layer depths used were 0.1, 0.2, 0.5 and 1.0 mm. For a thickness/depth ratio of 25%, the computed peak temperature increase is always less than T_0. The difference is significant for a shallow chromophore layer, and especially so when T_0 is less than 25 °C. For a thickness/depth ratio of 50%, the difference between computed peak temperature increase and T_0 is reduced (figure 4). Only when T_0 is 5 °C or less, and the chromophore layer thickness is 0.025 mm, is the computed peak temperature increase less than 60% of T_0.

For a chromophore layer thickness of 0.025 mm, centred at a depth of 0.1 mm, influence of SNR is significant. The computed peak temperature increase is greater than 65% of T_0 for SNR ratios of 100, 200 and 1000 (figure 5). When T_0 exceeds 25 °C, SNR becomes irrelevant. For an SNR of 1000, the computed peak temperature increase is essentially unaffected by the source temperature T_0.

The difference between the computed peak temperature increase and T_0 is greatest when T_0 is less than 25 °C, and SNR is less than 1000. At the extreme, the computed peak temperature increase/T_0 ratio is 12% when T_0 is 2.5 °C and SNR is 100.

In our calculations, the mean (first moment) of the deduced temperature increase distribution and $\int \Delta \boldsymbol{T}_{cg}\, \mathrm{d}z$ were predicted accurately (±10%), except for cases of: (i) thickness/depth ratio less than 10%, (ii) SNR below 10, or (iii) T_0 less than 5 °C. In these cases, the PPTR signal from the model ($\Delta \boldsymbol{S}$) is very small, and cannot be distinguished by the non-negatively constrained conjugate gradient algorithm from the background radiation level.

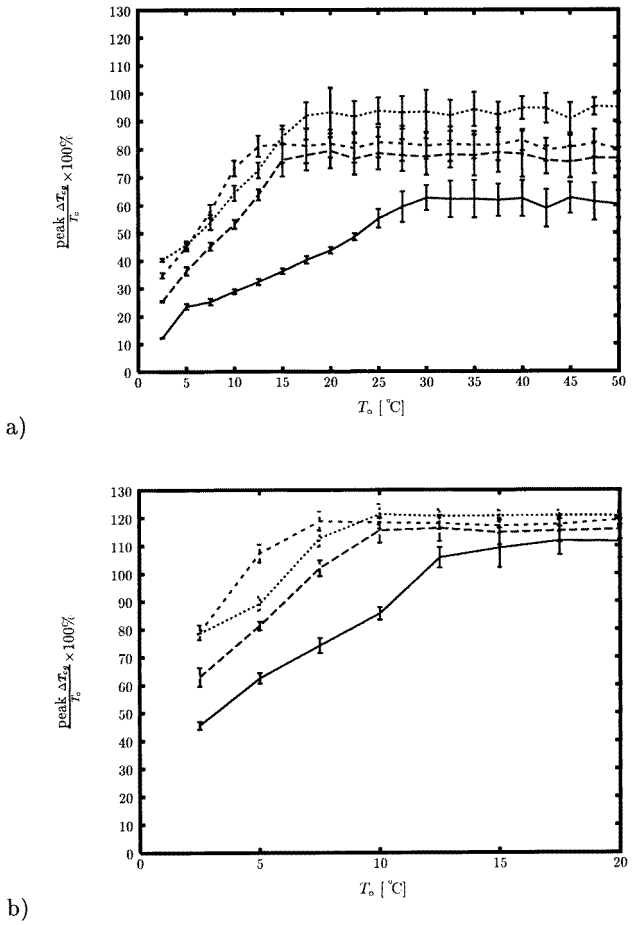

Figure 4. Ratio of computed peak temperature increase and T_0, for a chromophore layer at a depth of 0.1 mm (——), 0.2 mm (– – –), 0.5 mm (- - - -) and 1.0 mm (· · · · · ·). Thickness/depth ratios used: (*a*) 25% and (*b*) 50%. In (*b*), because computed peak temperature increases did not change appreciably for values of T_0 greater than 20 °C, these values are not displayed.

4. Discussion

It is to be expected that the non-negatively constrained conjugate gradient algorithm will perform poorly in cases where T_0 is low and SNR is high, since the PPTR signal from the model chromophore is obscured by the background radiation. To show why the thickness/depth ratio has a significant influence on the computed result, we use the singular value decomposition (SVD) of the kernel matrix, **K**. Thus

$$\mathbf{K} = \sum_{i=1}^{r} \delta_i \cdot \boldsymbol{\sigma}_i \cdot \boldsymbol{\tau}_i^{\mathrm{T}} \tag{9}$$

where $\boldsymbol{\sigma}_i$ and $\boldsymbol{\tau}_i$ are orthonormal left and right singular vectors of **K** and form a basis for the respective vector spaces containing the PPTR signal ($\Delta \boldsymbol{S}$) and temperature increase ($\Delta \boldsymbol{T}$); δ_i is the ith singular value of the PPTR kernel matrix **K**, where $\delta_i \geqslant \delta_j$ and $i < j$.

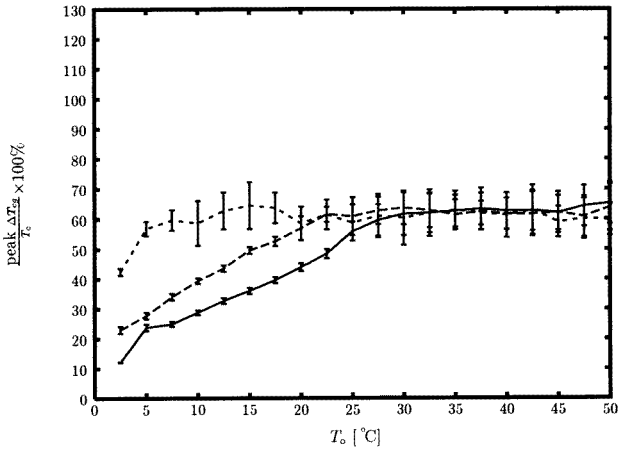

Figure 5. Computed peak temperature increase, as a percentage of T_0, when the SNR values are: 100 (——), 200 (– – –) and 1000 (- - - -). Chromophore layer depth is 0.1 mm, and thickness is 0.025 mm.

As $\{\boldsymbol{\tau}_i\}$ forms an orthonormal basis for the vector space spanning the simulated temperature increase ($\Delta \boldsymbol{T}_s$), a solution estimate ($\Delta \boldsymbol{T}_{svd}(k)$) may be expanded in terms of a variable number (k) of right singular vectors (equation (10))

$$\boldsymbol{T}_{svd}(k) = \sum_{i=1}^{i \leqslant k} (\boldsymbol{\tau}_i \cdot \Delta \boldsymbol{T}_s)\boldsymbol{\tau}_i. \tag{10}$$

Since the singular values, δ_i, rapidly decrease with increasing index i, ($\delta_i \approx A^{-i}$) where A is constant, the PPTR inversion problem is severely ill-posed and it is physically meaningless to include a large number of terms in the solution estimate (equation (10)). The maximum number of singular vectors in the solution estimate is determined by the SNR of the infrared detection system, which is limited by background photon noise. From Milner *et al* (1995a), when SNR is between 100 and 1000, k is ≈5–10, which is less than 8% of the rank of the kernel matrix.

An example of the effect of thickness/depth ratio on the computed temperature increase is given in figure 6, where $\Delta \boldsymbol{T}_{svd}(k)$ for various k are indicated. Solution estimates ($\Delta \boldsymbol{T}_{svd}$) are computed for superficial and deep chromophore layers of varying thickness. In all cases, greater accuracy of the solution estimate is obtained by increasing the number (k) of right singular vectors ($\boldsymbol{\tau}_i$) included. Accuracy of the solution estimate represented by a thin (0.1 mm) chromophore layer is best at superficial depths; inclusion of seven right singular values is sufficient for a reasonably accurate representation of the simulated temperature increase (figure 6(*a*)). In comparison, when the same chromophore layer is positioned 1 mm below the skin model surface and consequently the thickness/depth ratio is reduced, inclusion of 17 right singular vectors results in an estimate with significant error (figure 6(*b*)). Alternatively, when the thickness of the same chromophore layer is increased to 0.5 mm, the relative error of the solution estimate is improved significantly (figure 6(*c*)). Figure 6 illustrates a trend observed: when the thickness/depth ratio is less than 25% the computed peak temperature increase is always significantly less than T_0. Also, the thickness of the computed temperature increase is always larger than $\Delta \boldsymbol{T}_{ts}$.

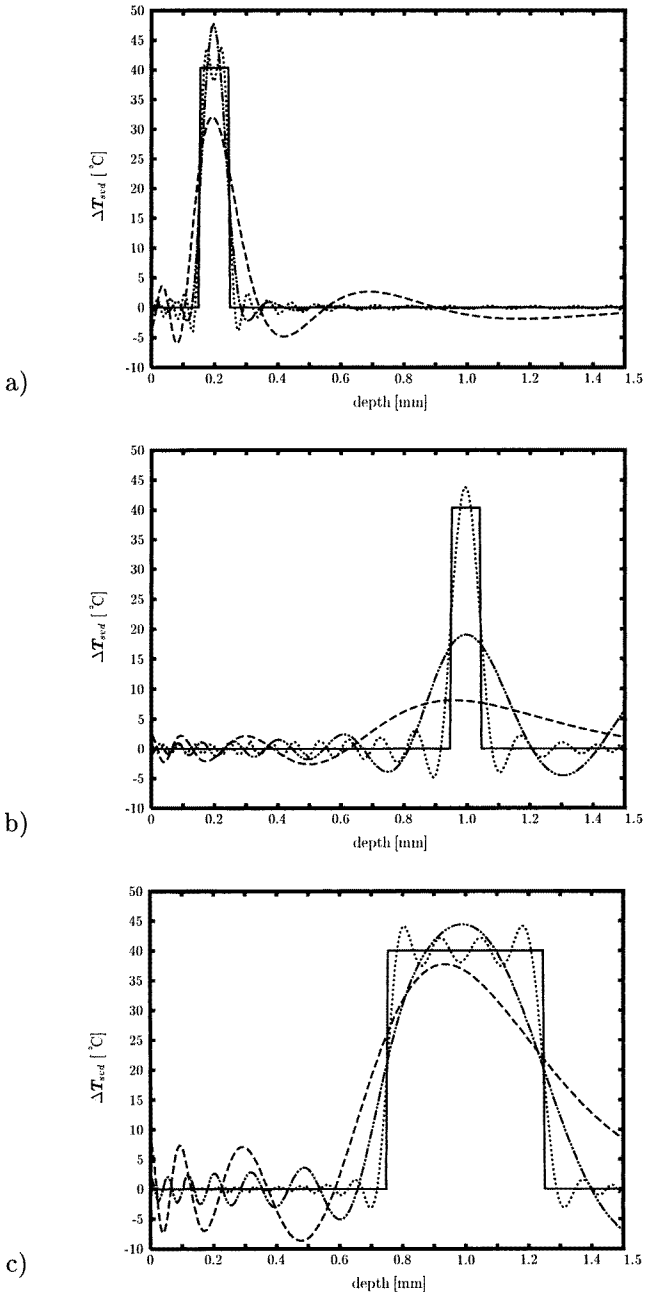

Figure 6. ΔT_{svd} calculated from a simulated temperature increase, where the chromophore layer has dimensions: (*a*) 0.1 mm thickness, depth 0.2 mm, (*b*) 0.1 mm thickness, depth 1.0 mm and (*c*) 0.5 mm thickness, depth 1.0 mm. Simulated temperature increase (——), 7 vectors (– – –), 17 vectors (— · · —) and 37 vectors (· · · · · ·).

Next we compute the relative error ($\epsilon(k)$, equation (11)) of the solution estimate ($\boldsymbol{T}_{svd}$), corresponding to a family of subsurface chromophore layers of varying thickness ($2r$)

and depth (z_m)

$$\epsilon(k) = \frac{\|\Delta \boldsymbol{T}_{svd}(k) - \Delta \boldsymbol{T}_s\|_1}{\|\Delta \boldsymbol{T}_s\|_1}. \tag{11}$$

In figure 7 $\epsilon(k)$ is depicted in a contour plot for various tophat shaped simulated temperature increase functions ($\Delta \boldsymbol{T}_{st}$). Values of $2r$ and z_m which give rise to temperature increase outside of the 0–1.5 mm depth range are not considered. Individual contour lines show a small oscillation that originates from the relatively few singular vectors used in the expansion (10) when calculating the relative error. A similar effect is observed when computing a Fourier expansion of an arbitrary function using relatively few sinusoidal terms. When the thickness/depth ratio is greater than 25%, the relative error ($\epsilon(k)$) is essentially constant.

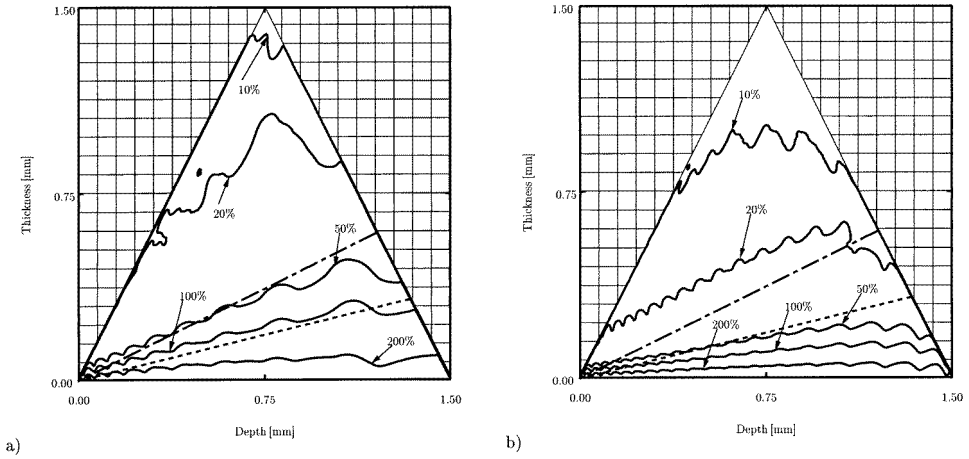

Figure 7. Relative error, $\epsilon(k)$, when (a) 10 and (b) 20 right singular vectors are used to represent various tophat shaped simulated temperature increase distributions ($\Delta \boldsymbol{T}_{st}$). Depth and thickness are specified by the axes, and contour lines are shown for solution estimates of 10%, 20%, 50%, 100% and 200%. The broken lines represent thickness/depth ratios of 25% (- - - -) and 50% (— · —). Values of thickness and depth not considered are indicated by the hatched regions.

In a PWS, the temperature distribution following pulsed laser irradiation decays approximately as an exponential with depth, commensurate with decreased fluence levels within blood (van Gemert *et al* 1986a). To simulate this, we describe temperature increase due to laser heated PWS blood vessels by an exponential distribution

$$\Delta \boldsymbol{T}_{es}(z) = \begin{cases} T_0 \exp\left(-\dfrac{z-d}{L_0}\right) & z \geqslant d \\ 0 & \text{otherwise.} \end{cases} \tag{12}$$

Here, L_0 is the exponential decay length, d is the minimum depth at which blood is found, T_0 is the peak temperature at $z = d$. Values for exponential decay length L_0 and depths d which introduced a discontinuity at $z = 1.5$ mm (i.e. $\Delta \boldsymbol{T}_{es}(z = 1.5 \text{ mm}) > 0.1T_0$) and significantly increased the relative error, $\epsilon(k)$, were not considered. The three-dimensional reconstruction of one PWS (Smithies *et al* 1997) indicates that the exponential temperature distribution is a reasonable approximation. There was a high concentration of vessels close to the surface, with the blood volume fraction approximately inversely proportional to depth. Following laser irradiation, the average temperature increase at each depth point will be similar to that described by equation (12).

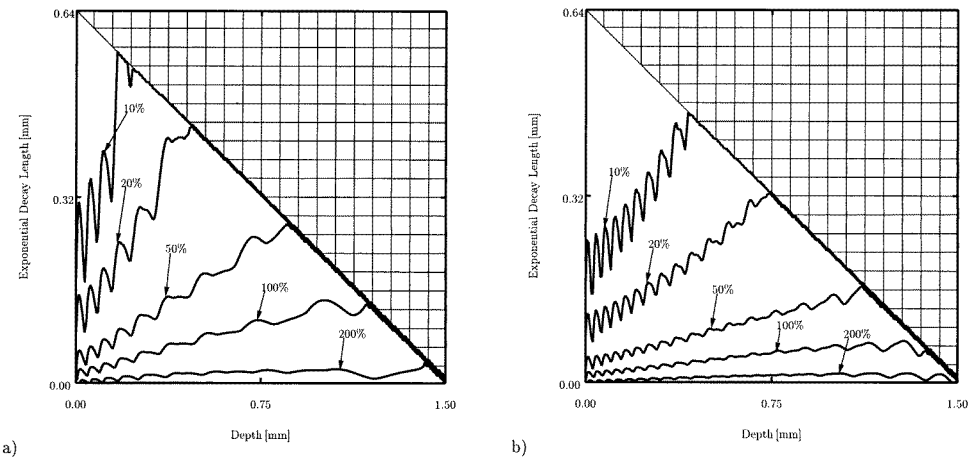

Figure 8. Relative error, $\epsilon(k)$, when (*a*) 10 and (*b*) 20 right singular vectors are used to represent various simulated temperature increase distributions ($\Delta \boldsymbol{T}_{es}$). Exponential decay length and minimum depth are specified by the axes and contour lines are shown for solution estimates of 10%, 20%, 50%, 100% and 200%. Values of exponential decay length and depth which were not considered are indicated by the hatched region.

In figure 8 $\epsilon(k)$ is depicted in a contour plot for various exponential shaped simulated temperature increase functions ($\Delta \boldsymbol{T}_{es}$). Individual contour lines show a small oscillation that originates from the relatively few singular vectors used in the expansion (10) when calculating the relative error. A similar effect is observed in figure 7. Relative error ($\epsilon(k)$) is essentially constant for a given exponential decay length/depth ratio.

5. Conclusion

Our results indicate the circumstances when PPTR may be used to accurately predict the thickness, depth and magnitude of temperature increase in the chromophore layer contained in a test material.

The mean (first moment) of the deduced temperature distribution and $\int \Delta T_{cg}(z)\,\mathrm{d}z$ were predicted accurately ($\pm 10\%$), except for cases of (i) thickness/depth ratio less than 10%, (ii) SNR below 10, or (iii) T_0 less than 5 °C.

When thickness/depth ratio is less than 25%, the difference between simulated and computed temperature increase is sufficiently large that the utility of the calculation is minimal. For these cases, the computed peak temperature increase is always significantly less than T_0, and the computed thickness of the chromophore layer is significantly larger, so that their product remains constant. Conversely, with a thickness/depth ratio greater than 25%, the computed peak temperature increase and chromophore layer thickness is much closer to the true value. Thus, PPTR alone cannot distinguish between a thin deep chromophore layer that reaches a high temperature and a relatively cool, thick and deep chromophore layer.

From the singular value decomposition of the kernel matrix, we verify results computed by application of the non-negatively constrained conjugate gradient algorithm, that the relative error is essentially constant for a particular thickness/depth ratio. The relatively small number of right singular vectors that may be used limits the accuracy of the computed temperature increase.

Acknowledgments

Institutional support from the Department of Energy, National Institutes of Health, and the Beckman Laser Institute and Medical Clinic Endowment is gratefully acknowledged (DJS, JSN). Support from research grants awarded from the Whitaker Foundation (WF-21025) (BST,TEM), and Institute of Arthritis and Musculoskeletal and Skin Diseases (1R29-AR41638-01A1 and 1R01-AR42437-01A1) at the National Institutes of Health (JSN,TEM) is also acknowledged. The contribution of Dennis M Goodman was performed under the auspices of a US Department of Energy grant to the Lawrence Livermore National Laboratory under contract W-7405-Eng-48.

References

Crostack H A, Jahnel W, Meyer E H and Pohl K J 1989 Recent developments in non-destructive testing of coated components *Thin Solid Films* **181** 295–304

Duck F A 1990 *Physical Properties of Tissue: A Comprehensive Reference Book* (London: Academic)

Favro L D, Ahmed T, Wang L, Wang X, Kuo P K, Thomas R L and Shepard S M 1993 Thermal wave imaging for aging aircraft inspection *Mater. Eval.* **51** 1386–9

Frank I E and Friedman J H 1993 A statistical view of some chemometrics regression tools *Technometrics* **35** 109–48

Goodman D M, Johansson E M and Lawrence T W 1993 On applying the conjugate gradient algorithm to image processing problems *Multivariate Analysis: Future Directions* ed C R Rao (Amsterdam: North-Holland)

Groetsch C W 1984 *The Theory of Tichonov Regularization for Fredholm Equations of the First Kind* (New York: Pitman)

Incropera F P and DeWitt D P 1985 *Fundamentals of Heat Transfer* (New York: Wiley)

Jacques S L, Nelson J S, Wright W H and Milner T E 1993 Pulsed photothermal radiometry of port-wine-stain lesions *Appl. Opt.* **32** 2439–46

Kimel S, Svaasand L O, Hammer-Wilson M, Schell M J, Milner T E, Nelson J S and Berns M W 1994 Differential vascular response to laser photothermolysis *J. Invest. Dermatol.* **103** 693–700

Long F H and Deutsch T F 1987 Pulsed photothermal radiometry of human artery *IEEE J. Quantum Electron.* **23** 1821–6

Long F H, Nishioka N S and Deutsch T F 1987 Measurement of the optical and thermal properties of biliary calculi using pulsed photothermal radiometry *Lasers Surg. Med.* **7** 461–6

Milner T E, Goodman D M, Tanenbaum B S, Anvari B and Nelson J S 1996b Noncontact measurement of thermal diffusivity in biomaterials using infrared imaging radiometry *J. Biomed. Opt.* **1** 92–7

Milner T E, Goodman D M, Tanenbaum B S, Anvari B, Svaasand L O and Nelson J S 1995b Imaging laser heated subsurface chromophores in biological materials: determination of lateral physical dimensions *Phys. Med. Biol.* **41** 31–44

Milner T E, Goodman D M, Tanenbaum B S and Nelson J S 1995a Depth profiling of laser-heated chromophores in biological tissues by pulsed photothermal radiometry *J. Opt. Soc. Am.* A **12** 1479–88

Milner T E, Smithies D J, Goodman D M, Lau A and Nelson J S 1996a Depth determination of chromophores in human skin by pulsed photothermal radiometry *Appl. Opt.* **35** 3379–84

Robertson C and Williams D 1971 Lambert absorption coefficients of water in the infrared *J. Opt. Soc. Am.* **61** 1316–20

Smithies D J, van Gemert M J C, Hansen M K, Milner T E and Nelson J S 1997 Three-dimensional reconstruction of port wine stain vascular anatomy from serial histological sections *Phys. Med. Biol.* **42** 1843–7

Stone M and Brooks R J 1990 Continuum regression: cross-validated sequentially constructed prediction embracing ordinary least squares, partial least squares, and principal components regression *J. R. Statist. Soc.* B **52** 237–69

van Gemert M J C, Welch A J and Amin A 1986 Is there an optimal treatment for port wine stains? *Lasers Surg. Med.* **6** 76–83

Vitkin I A, Wilson B C, Anderson R R and Prahl S A 1994 Pulsed photothermal radiometry in optically transparent media containing discrete optical absorbers *Phys. Med. Biol.* **39** 1721–44